Turbulent Characteristics of Saltation and Uncertainty of Saltation Model Parameters

Dongwei Liu[1], Masahide Ishizuka[2], Masao Mikami[3], Yaping Shao[4*]

[1]School of Ecology and Environment, Inner Mongolia University, China
liudw@imu.edu.cn
[2]Faculty of Engineering, Kagawa University, Japan
ishizuka@eng.kagawa-u.ac.jp
[3]Office of Climate and Environmental Research Promotion, Japan Meteorological Business Support Center, Japan
mikami@jmbsc.or.jp
[4]Institute for Geophysics and Meteorology, University of Cologne, Germany
yshao@uni-koeln.de

Abstract: It is widely recognized that saltation is a turbulent process, similar to other transport processes in the atmospheric boundary layer. Due to lack of high frequency observations, the statistic behavior of saltation is so far not well understood. In this study, we use data from the Japan-Australian Dust Experiment (JADE) to investigate the turbulent characteristics of saltation by analyzing the probability density function, energy spectrum and intermittency of saltation fluxes. Threshold friction velocity, u_{*t}, and saltation coefficient, c_0, are two important parameters in saltation models, often assumed to be deterministic. As saltation is turbulent in nature, we argue that it is more reasonable to consider them as parameters obeying certain probability distributions. The JADE saltation fluxes are used to estimate the u_{*t} and c_0 probability distributions. The stochasticity of these parameters is attributed to the randomness in friction velocity and threshold friction velocity as well as soil particle size.

Keywords: wind erosion; turbulent saltation; saltation intermittency; saltation model; threshold friction velocity; saltation coefficient; maximum likelihood

Highlight: We use data from a field experiment to investigate saltation by analysing the probability density function, energy spectrum and intermittency of saltation fluxes. We also estimate two key wind-erosion model parameters and their probabilistic distributions. It continues the line of treating saltation as a turbulent process and represents a progress towards deriving more general wind erosion models.

1. Introduction

It is well-recognised that saltation, the hoping motion of sand grains near the earth's surface, is a turbulent process [Bagnold, 1941]. However, early studies focused mainly on its "mean" behaviour. Most well-known is, for example, the Owen [Owen, 1964] saltation model which predicts that the vertically integrated saltation flux is proportional to u_* cubed, where u_* is friction velocity, defined as $u_* = \sqrt{\tau / \rho}$ with τ being surface shear stress (N m^{-2}) and ρ air density (kg m^{-3}). A dedicated investigation on turbulent saltation was conducted by Butterfield [1991], which revealed the significant variability of saltation fluxes concealed in conventional time-averaged data. Stout and Zobeck [1997] introduced the idea of saltation intermittency and pointed out that even when the averaged u_* is below the threshold friction velocity, u_{*t}, saltation can still intermittently occur. The latter authors emphasized on saltation intermittency caused by fluctuations of turbulent wind, but stochasticity of u_{*t} can also play a role. Turbulent saltation has attracted much attention in more recent years [e.g. McKenna Neuman et al. 2000; Davidson-

Arnott and Bauer, 2009; Sherman et al. 2017] and large-eddy simulation models have been under development to model the process [e.g. Dupond et al. 2013]. However, due to a lack of high-frequency field observations of saltation fluxes, the statistical behaviour of turbulent saltation is, to date, not well understood.

A related problem is how saltation can be parameterized in wind erosion models. For example, for dust modelling, it is important to quantify saltation, as saltation bombardment is a main mechanism for dust emission. In wind erosion models, u_{*t} is a key parameter which depends on many factors including soil texture, moisture, salt concentration, crust and surface roughness. In models, it is often expressed as

$$u_{*_t}(d;\lambda,\theta,s_l,c_r,\ldots) = u_{*_t}(d)\, f_\lambda(\lambda)\, f_\theta(\theta)\, f_{sl}(s_l)\, f_{cr}(c_r)\ldots \quad (1)$$

where $u_{*t}(d)$ is the minimal threshold friction velocity for grain size d [Shao and Lu, 2000]; λ is roughness frontal-area index; θ is soil moisture; s_l is soil salt content and c_r is a descriptor of surface crustiness; f_λ, f_θ, f_{sl} and f_{cr} are the corresponding correction functions. The corrections are determined semi-empirically, e.g., f_λ using the Raupach et al. [1993] scheme and f_θ the Fécan et al. [1999] scheme. The corrections f_{sl} and f_{cr} are so far not well known.

For homogeneous saltation, the saltation flux can be computed using the Kawamura [1964] scheme, here multiplied by the fraction of erodible surface area σ_f,

$$Q(d) = \begin{cases} \sigma_f c_o \dfrac{\rho}{g}\, u_*^3 \left(1-\dfrac{u_{*t}}{u_*}\right)\left(1+\dfrac{u_{*t}}{u_*}\right)^2 & u_* > u_{*t} \\ 0 & u_* \le u_{*t} \end{cases} \quad (2)$$

where d is particle diameter in sand particle size range and g is acceleration due to gravity. The saltation coefficient, c_0, is usually estimated empirically from field and/or wind-tunnel experiments. It falls between 1.8 and 3.1 according to Kawamura [1964], and is commonly set to 2.6 [White, 1979] in wind erosion models. The total (all particle sizes) saltation flux, Q, is a particle-size weighted average of $Q(d)$

$$Q = \int_{d_1}^{d_2} Q(d)\, p_s(d)\, \delta d \quad (3)$$

where d_1 and d_2 define the upper and lower limits of saltation particle size, respectively, and $p_s(d)$ is the soil particle size distribution. Observations show, however, c_0 varies considerably from case to case (e.g. Gillette et al. 1997; Leys, 1998), and as the data presented later in this paper show, for a given location, it may vary from day to day and even during a wind erosion event.

While wind-erosion modules built in numerical weather and global climate models [e.g. Shao et al. 2011; Kok et al. 2014; Klose et al. 2014] are in general more sophisticated than what is described above and include a dust emission scheme, the estimate of Q is essentially done using Equations (1) to (3) or similar. Thus, the estimates of u_{*t} and specification of c_0 are critical to wind-erosion and dust modelling.

In most wind erosion models, both u_{*t} and c_0 are treated as being deterministic. As saltation is turbulent, it is more rational to treat u_{*t} and c_o as parameters that satisfy certain probability distributions. Saltation intermittency also implies that u_{*t} and c_0 depend on the scale of averaging. Shao and Mikami [2005] noticed that u_{*t} for 10-minute averaged Q and 1-minute averaged Q are quite different. Namikas et al. [2003] and Ellis et al. [2012] have also noticed that averaging intervals of surface shear stress are important to quantifying sediment transport because both shear stress and saltation flux are turbulent.

Between 23 Feb and 14 Mar 2006, Ishizuka et al. (2008; 2014) carried out the Japan-Australian Dust Experiment (JADE) in Australia. In JADE, both u_* and Q, together with a range of atmospheric and soil surface quantities, were measured at relatively high sampling rates. The loamy sand soil surface at the JADE site was very mobile and thus the JADE data are representative to surfaces almost ideal for sand drifting. In this study, we analyse some aspects of the turbulent behaviour of saltation using the JADE measurements of saltation fluxes. In light of the analysis, we ask the question what the most likely values of u_{*t} and c_o are and how representative they are. We also estimate the probability distribution of the two parameters.

2. Data and Method for Parameter Estimation

2.1 JADE Data

Ishizuka et al. carried out JADE between 23 Feb and 14 Mar 2006 on an Australian farm at (33º50'42.4"S, 142º44'9.0"E). The size of field is about 1 km in the E–W direction and about 4 km in the N–S direction. A range of atmospheric variables, land surface properties, soil particle-size distributions and size-resolved sand and dust fluxes were measured. During the study period, 12 wind-erosion episodes were recorded. The dataset is particularly valuable in that particle size resolved sand and dust fluxes [Shao et al. 2011] were measured. The details of the experiments and datasets can be found in Ishizuka et al. [2008, 2014] and hence only a brief summary is given here.

In JADE, three Sand Particle Counters (SPCs) [Yamada et al. 2002] were used to measure saltation at the 0.05, 0.1 and 0.3 m levels with a sampling rate of 1 Hz. A SLD (Super Luminescent Diode) light source is used to detect particles flying through the light beam. The frequency of the input signal is 1-30 kHz, implying that particles moving with speed less than 30 m s^{-1} can be detected. A SPC measures the saltation of particles in the range of 39 - 654 µm in 32 bins with mean diameters of 39, 54, 69 µm etc. with irregular increment ranging between 15 and 23 µm. At each measurement height, the saltation flux density (M L^{-2} T^{-1}), q, is obtained as the sum of q_j (saltation flux for size bin j) for the 32 size bins, i.e.

$$q = \sum_{j=1}^{32} q_j \qquad (4)$$

The saltation flux, Q, is then estimated by integrating q over height, namely,

$$Q = \int q dz \qquad (5)$$

In computing Q, we assume $q = q_0 \exp(-az)$ with q_0 and a being fitting parameters from the measurements. Prior to the field experiment, the SPCs were calibrated in laboratory and during JADE, they were checked in a mobile wind-tunnel at the site and compared with other saltation samplers. But as q was measured only at three heights, the vertical resolution of q is relatively

poor and inaccuracies in the Q estimates are unavoidable, which we are unable to fully quantify. However, the profiles of q are well behaved and thus the inaccuracies in the absolute values of the Q estimates are not expected to be so large as to affect the conclusions of this study.

Q is computed using the SPC data at 1-second intervals. We denote its time series as Q_{1sec}. From Q_{1sec}, the one-minute averages, Q_{1min}, and 30-minute averages of saltation fluxes, Q_{30min}, are derived. All these quantities are also computed for individual particle size bins as

$$Q_j = \int q_j dz \qquad (5a)$$

Atmospheric variables, including wind speed, air temperature and humidity at various levels, as well as radiation, precipitation, soil temperature and soil moisture were measured using an automatic weather station (AWS). These quantities were sampled at 5-second intervals and their averages over 1-minute intervals were recorded. Two anemometers were mounted at heights 0.53 m and 2.16 m on a mast for measuring wind speed. Also available are the Monin-Obukhov length and sensible heat fluxes. From the wind measurements, surface roughness length z_0 and friction velocity u_* are derived, assuming a logarithmic profile (with stability correction) of the mean wind. The roughness length for the experiment site is estimated to be 0.48 mm.

Friction velocity is computed with 1-minute averaged wind data, denoted as u_{*1min}, and 30-minute averaged wind data, denoted as u_{*30min}. In atmospheric boundary-layer studies, there is no standard for how long one should average wind to "correctly" estimate u_*, but it is common to average over 10 to 30 minutes. But how long one averages depends on the purpose of the averaging. If u_* is used as a scaling velocity for the atmospheric boundary layer, e.g., as measure of turbulence intensity, it is necessary to average over a sufficiently large time interval to obtain a "constant" u_*. In this paper, u_* is a surrogate of shear stress, the variation of which drives that of saltation. Therefore, short averaging times are preferred, subject to that they are larger than the response time of aeolian flux to shear stress. Anderson and Haff (1988) and Butterfield (1991) suggested that this response time is of order of one second.

Observations of surface soil properties, including soil temperature and soil moisture, were made at 1-minute intervals. The surface at the JADE site was relatively uniform. A survey of ground cover over an area of 900 x 900 m^2 at the site was made on 11 March 2006. The area was divided into 9 tiles and surveyed along one transect of 300 m long in each tile. Photographs were taken every 5 m by looking down vertically to a point on the ground. Surface cover was estimated to be ~ 0.02 (see Appendix of Shao et al. 2011).

The wind erosion model, as detailed in Shao et al. (2011), is used for computing the saltation fluxes using the JADE atmospheric and surface soil measurements as input. The saltation model component is as described in Section 1, consisting of Equations (1) – (3). The fraction of erodible surface area, σ_f, used in Equation (1), is one minus the fraction of surface cover. The soil particle size distribution (psd), $p_s(d)$, required for Equation (3), is based on soil samples collected at the JADE site and analyzed in laboratory. The analysis was done using a Microtrac (Microtrac MT3300EX, Nikkiso Co. Ltd.), a particle size analyzer based on laser diffraction light scattering technology. Water was used for sample dispersion. Depending on the methods (pretreatment and ultrasonic vibration) used, the soil texture can be classified as sandy loam (clay 0.3%, silt 25% and sand 74.7%) or loamy sand (clay 11%, silt 35% and sand 54%). The sandy loam psd is used in this study, which has a mode at ~180 μm (see Shao et al. 2011, Fig. 5, Method A).

The default value of c_0 is set to 2.6, as widely cited in the literature [e.g. White, 1979] and the default value of u_{*t} is computed using Equation (1) with $u_{*t}(d)$ computed using the Shao and Lu [2000] scheme, f_λ using the Raupach et al. [1993] scheme, f_θ the Fécan et al. [1999] scheme, and f_{sl} and f_{cr} set to one. The frontal area index λ and soil moisture θ are both observed data from JADE.

2.2 Method for Parameter Estimation

Different choices of c_o and u_{*t} would lead to different model-simulated saltation fluxes which may or may not agree well with the measurements. By fitting the simulated saltation fluxes to the measurements, we determine the optimal estimates of c_0 and u_{*t} and the probability density function (pdf) of these parameters. The method based on the Bayesian theory is used for the purpose.

Suppose $\tilde{X} = (\tilde{x}_1, \tilde{x}_2, ..., \tilde{x}_n)$ is a measurement vector, with $\tilde{x}_i$ being the measured value at time t_i, and A is a model with a forcing vector F and model parameter vector β. Let the initial state of the system be i_0, then the modelled value of the system, $X = (x_1, x_2, \ldots, x_n)$, can be expressed as

$$X(\beta) = A(i_0, F; \beta) \tag{6}$$

The error vector is given by $E(\beta) = \tilde{X} - X$, here, fully attributed to β. Given $\tilde{X}$, the posterior parameter pdf, $p(\beta|\tilde{X})$, can be estimated from the Bayes theorem:

$$p(\beta|\tilde{X}) \propto p(\beta)\, p(\tilde{X}|\beta) \tag{7}$$

where $p(\beta)$ is the prior parameter pdf and $p(\tilde{X}|\beta)$ the likelihood. If $p(\beta)$ is given, then the problem of finding $p(\beta|\tilde{X})$ reduces to finding the maximum likelihood. Assuming the error residuals are independent and Gaussian distributed with constant variance, σ^2, the likelihood can be written as

$$p(\tilde{X}|\beta) = \prod_{i=1}^{n} \frac{1}{\sqrt{2\pi}\sigma} \exp\left(-\frac{(x_i - \tilde{x}_i)^2}{2\sigma^2} \right) \tag{8}$$

In this case, maximizing the likelihood is equivalent to minimizing the error, i.e.,

$$R^2(\beta) = \min \sum_i (x_i - \tilde{x}_i)^2 \tag{9}$$

The solution of Equation (9) gives an optimal (i.e. with maximum likelihood) estimate of mean β. This is the popular least-squares method. A disadvantage of the method is that it assumes a Gaussian posterior parameter pdf and the computing the β variance requires the pre-knowledge of the accuracy of the data.

As an alternative, the approximate Bayesian computation (ABC) method has been proposed [e.g. Vrugt and Sadegh, 2013]. It is argued that a parameter value β^* should be a sample from

$p(\beta|\tilde{X})$ as long as the distance between the observed and simulated data is less than a small positive value

$$\rho(\beta^*) = \left| X(\beta^*) - \tilde{X} \right| \leq \varepsilon \qquad (10)$$

This procedure provides explicitly an estimate of parameter pdf for given dataset. The ABC method is numerically simple: from a prior pdf (e.g. uniform) of β a β^* is stochastically generated and the model is run. If Equation (10) is satisfied, then β^* is accepted or otherwise rejected. This procedure is repeated and the a-priori pdf of β is mapped to a posterior pdf of β. The ABC method has the disadvantage though that it is numerically inefficient. More efficient techniques based on the same principle exist, e.g., Markov Chain Monte Carlo Simulation [Sadegh and Vrugt, 2014]. In this study, we apply the Differential Evolution Adaptive Metropolis (DREAM) algorithm proposed by Vrugt et al. (2011) for estimation of hydrologic model parameters. The algorithm integrates Differential Evolution [Storn and Price, 1997] and self-adaptive randomized subspace sampling to accelerate a Markov Chain Monte Carlo simulation. A full description of the DREAM algorithm is beyond the scope of our study. Interested readers should refer to the above cited references for details.

3. Statistical Features of Saltation

3.1 Time Series

To provide an overview of the dataset used in this study. Fig. 1a shows the time series of Q_{1min} and u_{*1min}, and Fig. 2 Q_{30min} and u_{*30min}. During the 20-day period, aeolian sand drift occurred almost every day at the site according to the field logging book, but only 12 events were recorded using the SPCs. Saltation fluxes were not measured on Day 55, 58, 59, 64 and then Day 66 to 70, due to either instrument maintenance or use of the SPCs for other purposes (e.g. wind-tunnel experiments). The figures show that both Q and u_* fluctuate significantly and saltation is turbulent. Fig. 1b shows an enlarged plot of the Q_{1min} and u_{*1min} time series for Day 61 and 62. At the JADE site, u_{*t} was about 0.2 m s^{-1}. On Day 61, u_* was mostly larger than this value and saltation was almost continuous, while on Day 62, u_* was close to this value and weak saltation occurred frequently also when u_* was below 0.2 m s^{-1}. Fig. 2b is as Fig.1b, but for Q_{30min} and u_{*30min}. A comparison of Fig. 1b and Fig. 2b reveals that the amplitude of the Q_{1min} fluctuations is several times of that of the Q_{30min} fluctuations. A strong correlation between the time series of Q_{30min} and u_{*30min} can be directly seen in Fig. 2b.

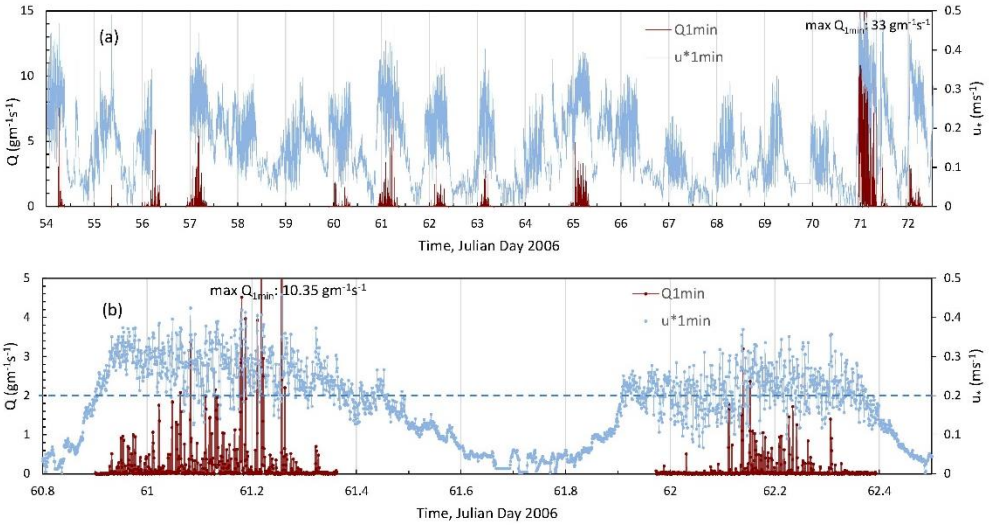

Figure 1: (a) Observed time series of 1-min averaged saltation flux, Q_{1min} (g m^{-1} s^{-1}), and friction velocity, u_{*1min} (m s^{-1}), for the JADE study period; (b) an enlarged plot of (a) for the erosion events on Day 61 and 62. Note that the axes in (b) have different scales than in (a).

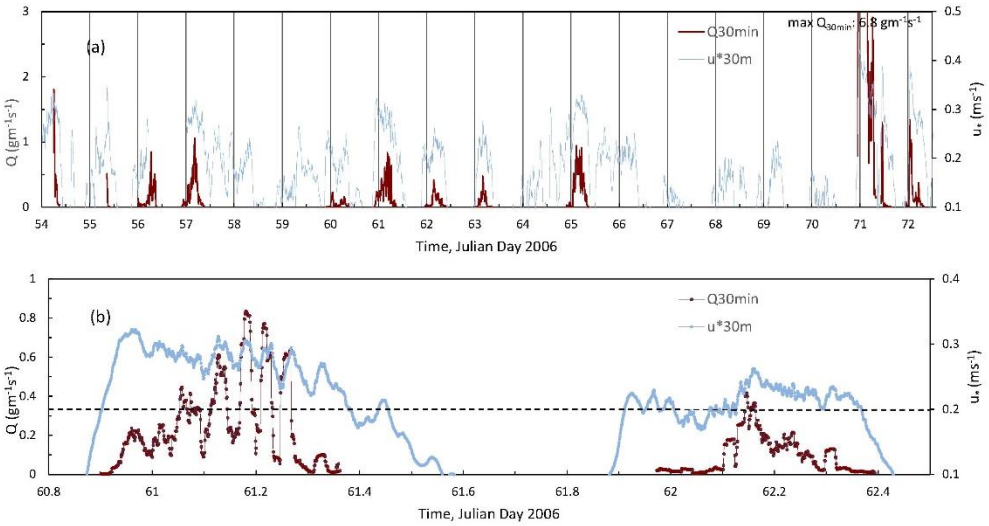

Figure 2: As Fig. 1, but for running means over 30-min intervals.

In Fig. 3a, b and c, Q is plotted against u_*^3. Several interesting features can be identified. For the majority of the points, the $Q \sim u_*^3$ relationship appears to hold, but this relationship can vary significantly even for the same data set from event to event. For example, large differences exist between days 70 and 71 (denoted D70-71, an event of intensive wind erosion) and Day 72 (a day of weak wind erosion), as seen in both Fig. 3a and Fig. 3b. There may be many likely reasons for the differences the $Q \sim u_*$ relationship but the most conspicuous are differences in atmospheric turbulence (e.g., gustiness) and time-varying surface conditions (e.g. particle sorting and aerodynamic roughness). Fig. 3d shows the time series of (u_{*1min}–u_{*30min}), a measure of turbulent fluctuations. It is seen that saltation is associated with not only high surface shear stress but also high shear stress fluctuations. The large difference in the $Q \sim u_*$ relationship between D70-71 and D72 (Fig. 3b) is probably attributed to the strong differences in turbulent fluctuations (Fig. 3d): D70-71 was a hot gusty day with top (2 cm) soil temperature reaching 53^{o}C, while D72 was cooler and less gusty with soil temperature 5^{o}C lower. Also hysteresis is

observed in the Q~u_* relationship, as shown in Fig. 3c, using D71 and D72 as example. Fig. 3d shows that for all three events selected (D70-71, D71 and D72), saltation has a relatively short (0.5 to 2 hours) strengthening phase, followed by a longer weakening phase. During an erosion event, for the same u_*, saltation is stronger in the strengthening than in the weakening phase. An examination of Fig. 3d suggests that the hysteresis cannot be simply attributed to the intensity of turbulence. We speculate that it is probably more related to flow-saltation feedbacks (e.g. stronger splash entrainment in the strengthening phase) and the modification of surface aerodynamic conditions (e.g. particle sorting and reduced surface roughness Reynolds number).

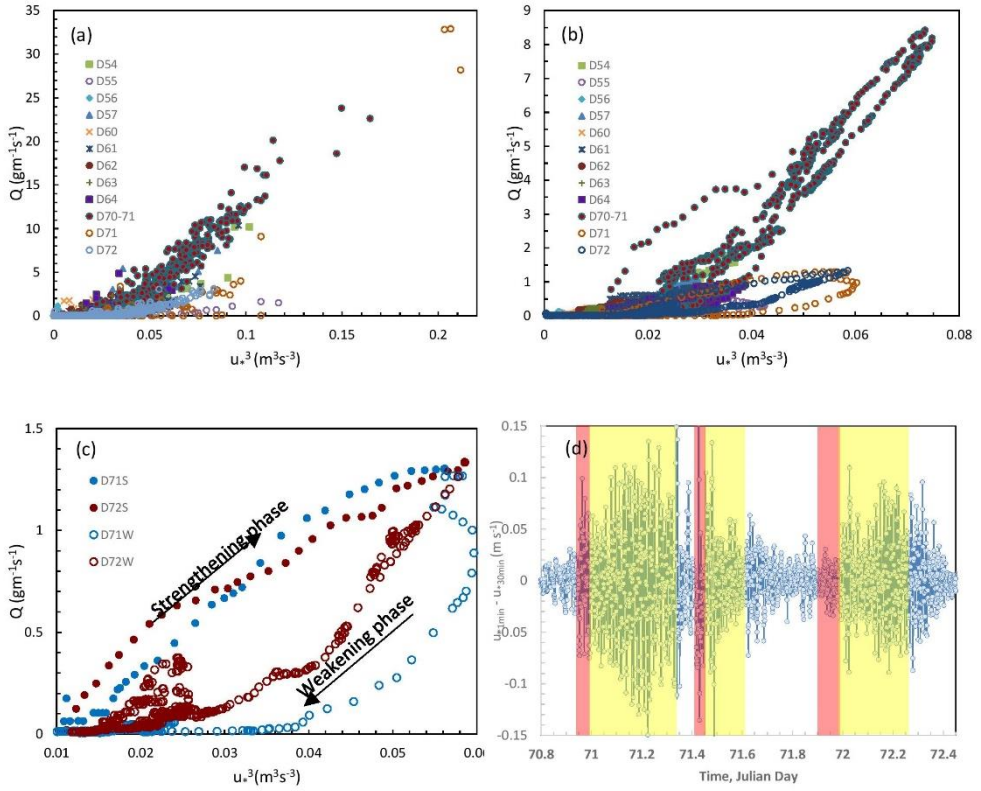

Figure 3: (a) Saltation flux, Q (g m^{-1} s^{-1}), plotted against friction velocity, u_*^3 (m^3 s^{-3}), for 1-minute averages; (b) As (a), but for 30-minute averages; (c) As (b), but enlarged to illustrated saltation hysteresis on D71 and 72; D71S/72S denote the strengthening and D71W/72W the weakening phase of the D71/72 event; (d) Time series of u_* derivations, given by (u_{*1min}–u_{*30min}), for D70-71, D71 and D72. The strengthening phase is marked red and the weakening phase yellow.

3.2 Probability Density Function of Saltation Fluxes

How well the saltation model performs, whether u_{*t} and c_o are universal and how they are probabilistically distributed must depend on the turbulent properties of saltation. As the JADE saltation fluxes are sampled at 1 Hz, we can use these data to examine (to some degree) the statistical behavior of saltation. In Fig. 4, the pdfs of the saltation fluxes for different particle size groups are plotted, computed using Q_{1sec} and Q_{1min}. It is seen that the pdfs generally behaves as

$$p(Q) \propto Q^{-\alpha} \qquad (11)$$

In case of Q_{1sec}, there seems to be a distinct change in α at a critical value of $Q_c \sim 3$ g m^{-1} s^{-1}, with $\alpha \sim 1$ for $Q < Q_c$ and $\alpha \sim 4$ for $Q > Q_c$. The pdfs derived from Q_{1min} appear to follow the basic functional form of Equation (11). Again, α is about 1 and tends to be larger for large Q values. Fig. 4 shows that the pdfs of Q depend significantly on the interval of time averaging, i.e., after averaging, smaller saltation fluxes become more frequent. This is because the time series of Q_{1sec} is more intermittent (see also Fig. 6).

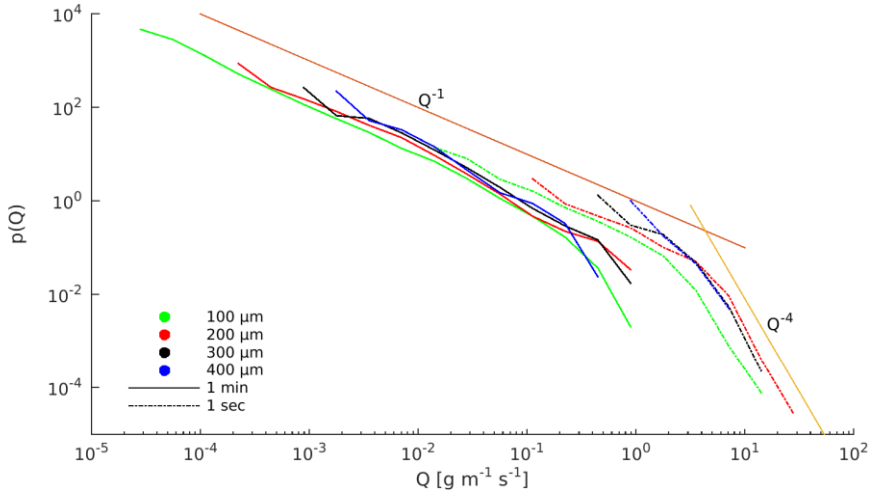

Figure 4: Probability density functions of Q_{1sec} (solid lines) and of Q_{1min} (dashed lines) for four different particle sizes. Two additional lines $p(Q) \sim Q^{-1}$ and Q^{-4} are drawn as reference.

The pdfs of Q_{1sec} and Q_{1min} integrated over all particles are shown in Figure 5b. Again, the pdfs show the general behavior of $p(Q) \sim Q^{-1}$. In theory, $p(Q)$ can be derived from the pdf of u_*, $p(u_*)$. From Equation (2), we have

$$\frac{dQ}{du_*} = c_0 \frac{\rho}{g}\left(3u_*^2 + 2u_* u_{*t} - u_{*t}^2\right) \quad \text{for} \quad u_* > u_{*t} \tag{12}$$

This can be used to obtain

$$p(Q) = \begin{cases} p(u_*)\dfrac{du_*}{dQ} & \text{for} \quad u_* > u_{*t} \\ 0 & \text{for} \quad u_* \le u_{*t} \end{cases} \tag{13}$$

Fig. 5a shows the $p(u_*)$ estimated from u_{*1min} together with the fitted Weibull distribution. For the fitting, emphasis is made to ensure that $p(u_*)$ for $u_* > 0.2$ ms^{-1} is best approximated. Fig. 5b shows the $p(Q)$ estimated from Q_{1min}. We computed $p(Q)$ using Equation (13) with the fitted $p(u_*)$, assuming $u_{*t} = 0.2$ ms^{-1} and $c_0 = 2.6$. It is seen that the observed and modelled $p(Q)$ have qualitative similarities (namely $p(Q)$ decreases with increasing Q) but using Equations (12) and (13) we cannot well reproduce the observed $p(Q)$. For example, the model fails to predict the lowly frequent strong saltation fluxes and fails to predict the highly frequent weak saltation occurring when u_* is below the specified threshold. Tests using several smaller u_{*t} values (0, 0.05 and 0.1). With smaller u_{*t} values, the highly frequent weak saltation fluxes are better reproduced, but fra from satisfactory.

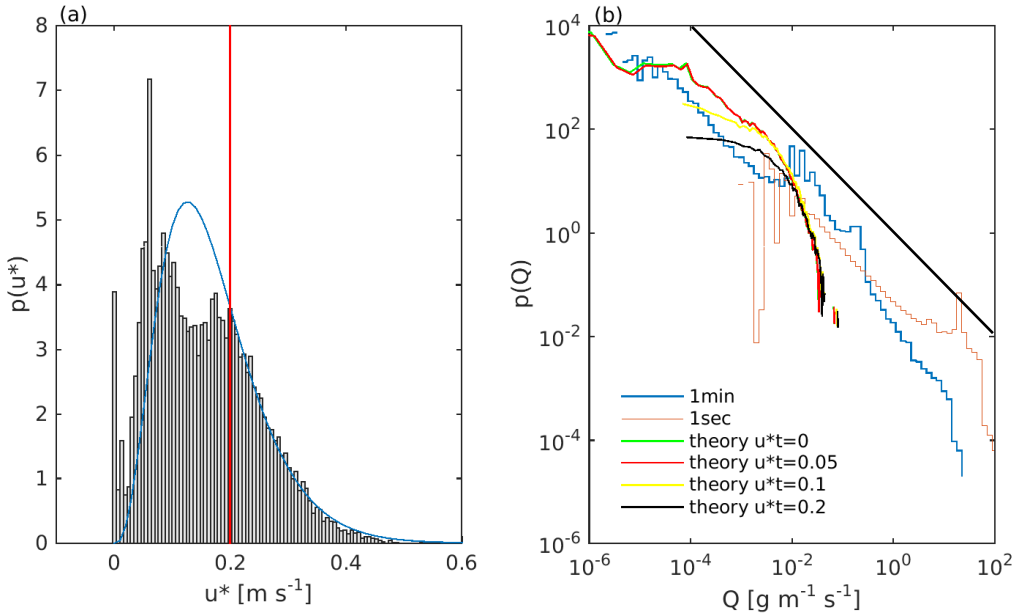

Figure 5: (a) Probability density functions of friction velocity, $p(u_*)$, plotted against u_* (bars). To compute $p(u_*)$, u_{*1min} is used; a Weibull distribution (blue line) is fitted to $p(u_*)$; the red line marks the assumed threshold friction velocity. (b) Probability density function of Q, $p(Q)$, estimated using Q_{1min} (blue) and Q_{1sec} (dark red) and using Equation (13) assuming several u*t values (u_{*t} = 0.0 m s^{-1}, green; 0.05 m s^{-1}, red; 0.1 m s^{-1}, yellow; 0.2 m s^{-1}, black). The $p(Q) \sim Q^{-1}$ line is also drawn for comparison.

3.3 Saltation Intermittency

Following Stout and Zobeck [1997], the intermittency of saltation, γ, is defined as the fraction of time during which saltation occurs at a given point in a given time period. It should be pointed out that as saltation is a turbulent process, saltation intermittency describes only the behaviour of the process at $u_* \sim u_{*t}$, i.e., saltation intermittency is merely a special, although important, case of turbulent saltation. Several formulations of γ are possible. Stout and Zobeck [1997] assumed that saltation occurs only in time windows when u_* exceeds u_{*t}. Therefore, if $p(u_*)$ is known, then γ for a given u_{*t} can be estimated as

$$\gamma_a(u_{*t}) = 1 - \int_0^{u_{*t}} p(u_*)du_* \qquad (14a)$$

Stout and Zobeck [1997] used the counts per second of sand impacts on a piezoelectric crystal saltation sensor as a measure of saltation activity and found that γ_a rarely exceeded 0.5.

In Equation (14a) u_{*t} is fixed and thus saltation intermittency is attributed entirely to the fluctuations of u_*. In reality, u_{*t} also fluctuates and satisfies certain pdfs (Raffaele et al., 2016). In analogy to Equation (14a), γ for a given u_* can be estimated as

$$\gamma_b(u_*) = 1 - \int_{u_*}^{\infty} p(u_{*t})du_{*t} \qquad (14b)$$

More generally, we can define saltation intermittency as

$$\gamma_c = \int_0^{\infty}\left[1 - \int_0^{u_{*t}} p(u_*)du_*\right]p(u_{*t})du_{*t} = \int_0^{\infty}\gamma_a(u_{*t})p(u_{*t})du_{*t} \qquad (14c)$$

or

$$\gamma_c = \int_0^{\infty}\left[1 - \int_{u_*}^{\infty} p(u_{*t})du_{*t}\right]p(u_*)du_* = \int_0^{\infty}\gamma_b(u_*)p(u_*)du_* \qquad (14d)$$

Equations (14c) and (14d) reduce to Equation (14a) in case of $p(u_{*t}) = \delta(u_{*t})$ and to Equation (14b) in case of $p(u_*) = \delta(u_*)$, respectively.

The computation of saltation intermittency function $\gamma_a(u_{*t})$ is done by integrating $p(u_*)$ (Fig. 5a) to fixed value of u_{*t}. In Fig. 6a, γ_a as function of u_{*t} is plotted. The behaviour of $\gamma_a(u_{*t})$ is as expected: it is one at $u_{*t} = 0$ and decreases to zero at about $u_{*t} = 0.5$ ms^{-1} as in the case of JADE, u_* rarely exceeded this value. For $u_{*t} = 0.2$ ms^{-1}, γ_a is 0.35, comparable with the result of Stout and Zobeck (1997) who reported an intermittency of 0.4. As $p(u_{*t})$ is not known, Equation (14b) cannot be used directly, but we can compute $\gamma_b(u_*)$ using the JADE data. First, it is computed using Q_{1min}. This is done by selecting a fixed u_* say u_{*c}, and counting the time fraction, T_{u*}, which satisfies $|u_* - u_{*c}| < \delta$ (used is δ = 0.05 ms^{-1}) and the time fraction, T_{Q1min}, which satisfies $|u_* - u_{*c}| < \delta$ and $Q_{1min} > 0$. By definition, saltation intermittency is T_{Q1min}/T_{u*} as plotted in Fig. 6a. It is seen that for Q_{1min}, $\gamma_b(u_*)$ increases from about 0.6 at $u_* \sim 0.1$ ms^{-1} to about one at $u_* = 0.3$ ms^{-1}. This shows that in JADE a considerable fraction of the saltation fluxes was recorded at u* below the perceived threshold friction velocity (about 0.2 ms^{-1}), saltation is more intermit under weak wind conditions and becomes non-intermittent for $u_* >$ 0.3 ms^{-1}. The increase of $\gamma_b(u_*)$ with decreasing u_* for $u_* < 0.1$ ms^{-1} is however unexpected. The expected $\gamma_b(u_*)$ for small u_* is as depicted using the dashed line. A likely reason for the unexpected behaviour of $\gamma_b(u_*)$ is that during a wind erosion event, grains in saltation may continue to hop even when u_* is temporarily reduced to small values. The uncertainty in the data also needs to be considered, as the sample size for determining the ratio T_{Q1min}/T_{u*} becomes smaller. More complete datasets are required to answer these questions. Finally, γ_c is computed by using Equation (14d) and is found to be around 0.73. For the one-second case, we cannot plot γ_b as a function of u_*, because u_* is not available at such high frequency. We computed γ_c for individual particle size groups (Fig. 6b) using Q_{1sec}, Q_{1min} and Q_{30min}, which is the time fraction of saltation for a given particle size, d, during the saltation event. It is found that $\gamma_c(d)$ decreases with d, i.e., the saltation of larger particles is more intermittent. Also, $\gamma_c(d)$ increases with increased averaging time intervals, implying that the small scales features of turbulence play an important role in intermittent saltation.

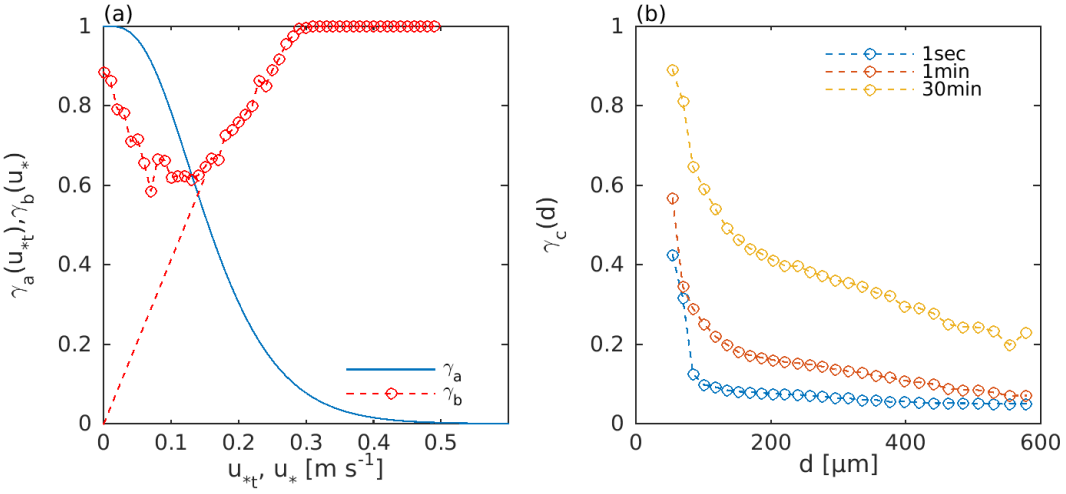

Figure 6: (a) Saltation intermittency function $\gamma_a(u_{*t})$, and $\gamma_b(u_*)$. See text for more details. (b) γ_c as a function of particle size for Q_{1sec}, Q_{1min} and Q_{30min}.

3.4 Spectrum of Saltation Fluxes

Spectral analysis is a widely used for characterising the variations of a stochastic process on different scales. Using the JADE data, we computed the power spectrum of saltation fluxes, $P_Q(f)$ at frequency f, and of friction velocity, $P_{u*}(f)$, using a non-uniform discrete Fourier transform. For comparison, the power spectra are normalized with the respective variances of the signal. In atmospheric boundary-layer studies, the spectra of various turbulence quantities have been thoroughly investigated (Stull, 1988). Examples for spectra of Reynolds shear stress can be found in McNaughton and Laubach (2000). Fig. 7 shows $P_Q(f)$ and $P_{u*}(f)$ (Fig. 7a) as well their co-spectrum (Fig. 7b). $P_Q(f)$ is computed using both Q_{1sec} and Q_{1min}, and $P_{u*}(f)$ with u_{*1min}. It is seen that the power spectra of Q and u_* have qualitatively very similar behaviour. Both have a maximum at about 10^{-5} Hz, a minimum at about 10^{-4} Hz and another peak at about 2×10^{-3} Hz. The maximum at 10^{-5} Hz is related to the diurnal patterns and changing synoptic events, which drive the wind erosion episodes, the minimum at 10^{-4} Hz is due to the lack of turbulent winds at the time scale of several hours, while the peak at 2×10^{-3} Hz is caused by the minute-scale gusty winds/large eddies in turbulent flows. Also the Q-u_* co-spectrum shows that Q and u_* are most strongly correlated on diurnal/synoptic and gust/large-eddy time scales. $P_Q(f)$ computed using Q_{1sec} reveals again the peaks at 10^{-5} Hz and at 2×10^{-3} Hz. The power of the Q spectrum then decreases with frequency. As the sampling rate of saltation flux is limited to one second in this study, the features of $P_Q(f)$ at frequencies larger than 0.5 Hz are not resolved.

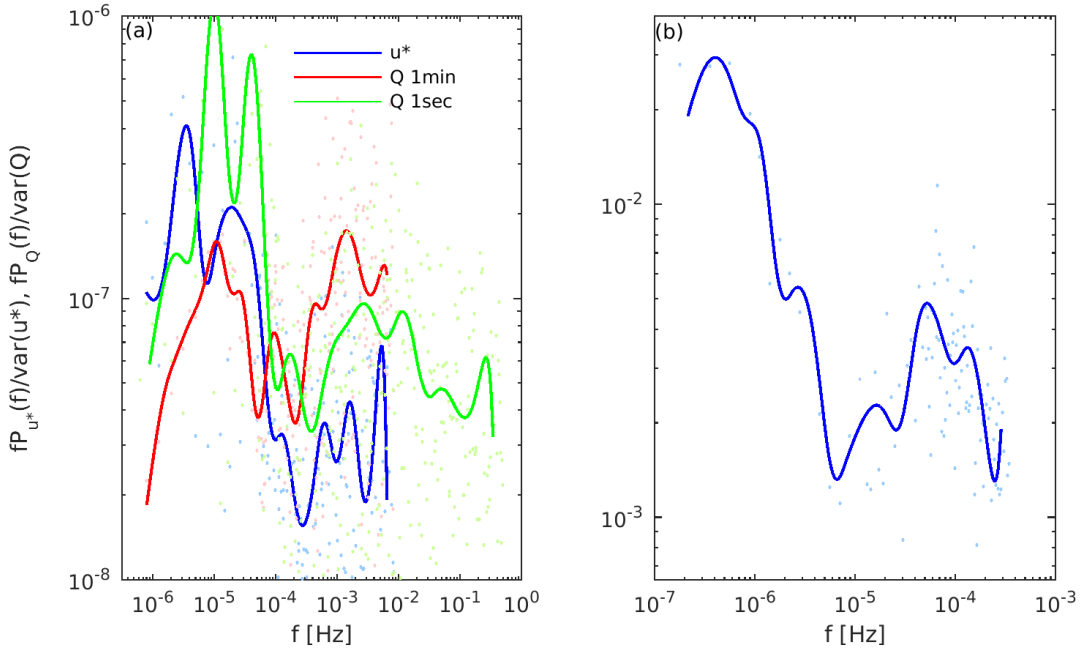

Figure 7: (a) Normalized power spectrum of u_*(blue) computed with u_{*1min}, together with the normalized power spectrum of saltation flux computed with Q_{1min} (red) and Q_{1sec} (green). (b) Normalized Q-u_* co-spectrum, computed using with Q_{1min} and u_{*1min}. In both (a) and (b), dots are unsmoothed spectra, and curves are smoothed spectra.

4. Estimates of Saltation Model Parameters

Given the turbulent nature of saltation, it is rational to treat u_{*t} and c_0 in the saltation model as parameters obeying certain probability distributions. To examine the behavior of these parameters, we introduce two coefficients r_{c0} and $r_{u*t,}$ and multiply them respectively by the "theoretical" values of c_0 and u_{*t} in Equation (2), i.e.

$$u_{*t} = r_{u*t} u_{*t,theory}$$
$$c_0 = r_{c0} c_{0,theory}$$

As introduced in Section 1, we assumed $c_{0,\,theory} = 2.6$ and computed $u_{*t,\,theory}$ using Equation (1) with observed soil moisture and fraction of cover. The two coefficients r_{c0} and r_{u*t} are varied to generate a model estimate of Q using Equations (2) and (3) with observed u_*. The probability distributions of r_{c0} and r_{u*t} are estimated using the following techniques. Let us denote the time series of the modelled saltation flux as $Q_{M,i,}$ (i=1,N) and of the corresponding measurement $Q_{D,i}$. The absolute error, δQ_A, and Nash coefficient, I_{Nash}, are used as measures for the goodness of the agreement between the model and the measurement. They are defined as,

$$\delta Q_A = \frac{1}{N}\sum |a_i|$$
$$I_{Nash} = (1 - \sum a_i^2 / \sum b_i^2)$$

with

$$a_i = Q_{M,i} - Q_{D,i}$$

$$b_i = Q_{M,i} - \frac{1}{N}\sum Q_{M,i}$$

$$c_i = \begin{cases} a_i / Q_{M,i} & Q_{M,i} \neq 0 \\ 0 & \text{else} \end{cases}$$

The prior pdfs of r_{c0} and r_{u*t} are assumed to be uniform. In the numerical experiment, we randomly generate r_{c0} and r_{u*t} and seek their values, such that $\delta Q_A \leq \varepsilon$ and $I_{Nash} > \eta$. These experiments are repeated for Q_{1min} and Q_{30min}. The plots of δQ_A and I_{Nash} as functions of r_{c0} and r_{u*t} show that for certain values of r_{c0} and r_{u*t}, the above conditions are satisfied. Fig. 8 shows that for Q_{1min}, the best simulation is achieved with r_{c0} = 1.23 and r_{u*t} = 1.05, while for the Q_{30min}, with r_{c0} = 0.94 and r_{u*t} = 0.91. This suggest that the "optimal" estimates of u_{*t} and c_0 are close to the corresponding theoretic values, but are dependent on the time averaging intervals, with both u_{*t} and c_0 being larger for shorter averaging intervals.

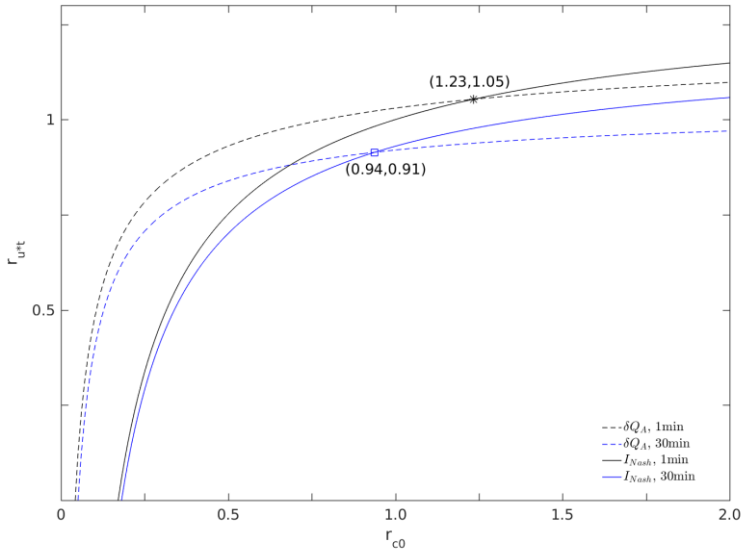

Figure 8: δQ_A and I_{Nash} are both functions of r_{c0} and r_{u*t}. Along the dashed curves, the condition $\delta Q_A = \min$ is satisfied and along the solid curves the condition $I_{Nash} = \max$ is satisfied. The curves are estimated with both Q_{1min} and Q_{30min}.

The parameter pdfs $p(r_{u*t})$ and $p(r_{c0})$ are estimated with the DREAM algorithm, again using the absolute error and the Nash coefficient as goodness of agreement between the model simulated and measured saltation fluxes. The results are shown in Fig. 9. All pdfs are fitted to a Γ-distribution. As seen in Fig. 9a and 9c, the most frequent r_{u*t} values are respectively 1.12 and 1.04 for Q_{1min} and Q_{30min}, close to the estimates of 1.05 and 0.91 found in Fig. 8. For Q_{1min}, r_{u*t} is ~1.12 ± 0.2 and for Q_{30min} ~1.04 ± 0.3. This implies that sometimes saltation occurs when u_* is below the theoretical u_{*t} value and sometimes saltation does not occur even when u_* is above it, as already seen in Fig. 6a. In the case of $p(r_{c0})$ (Fig. 9c and 9d), the most frequent values of r_{c0} for Q_{1min} and Q_{30min} are, respectively, 1.04 and 0.92, close to the optimal estimates of 1.23 and 0.94 shown in Fig. 8. But r_{c0} varies over a wide range, for instance, for Q_{30min} between 0.5 and 5, i.e., c_0 is a rather stochastic parameter.

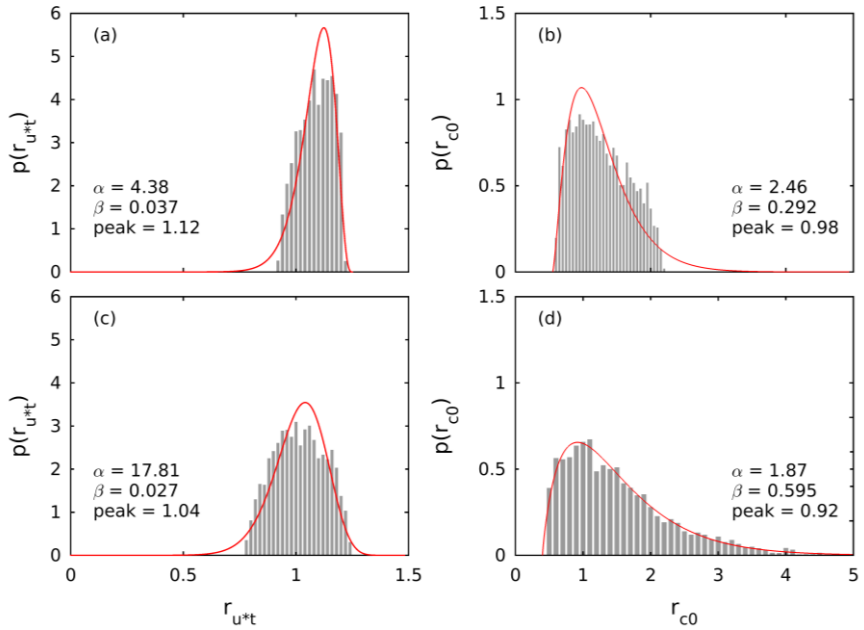

Figure 9: (a) Parameter pdf $p(r_{u*t})$ for 1-min averaged saltation fluxes; (b) as (a), but for $p(r_{c0})$; (c) and (d), as (a) and (b), but for 30-min averaged saltation fluxes.

In nature, many factors influence sediment transport, but the stochasticity of the parameters is determined primarily by the turbulent fluctuations of friction velocity (or surface shear stress), the randomness of threshold friction velocity, and soil particle size distribution (representing particle response to forcing). Studies have shown, for instance, that small changes in soil moisture can have large influences on saltation [Ishizuka et al. 2008] and soil moisture in the very top soil layer can vary significantly over relatively short time periods. Over the period of 18 days during JADE soil moisture in the top 0.05 m layer varied between 0.02 and 0.04 m^3m^{-3} (4 and 8% in relative soil moisture, assuming a saturation soil moisture of 0.5 m^3 m^{-3}). In this study, the influence of soil moisture on saltation is accounted for via Equation (1) using the soil moisture measurements in the top 0.05m layer (see also Fig. 4a in Shao et al. 2011). While measured soil moisture is used in the wind erosion model, the randomness associated with its spatial-temporal variations is not, which is most likely reflected in the stochasticity of u_{*t}.

The stochasticity of c_0 arises because saltation fluctuates, depending on turbulence and particle size. To demonstrate this, we divided the time series of the saltation fluxes into two subsets, one with $Q_{D,i} \leq 3$ g m^{-1} s^{-1} representing weak saltation and one with $Q_{D,i} > 3$ g m^{-1} s^{-1} representing significant saltation. This separation is arbitrary but sufficient for making the point that c_0 depends on u_*, also a measure of turbulence intensity. The parameter pdfs, $p(r_{u*t})$ and $p(r_{c0})$, for the subset $Q_{D,i} \leq 3$ g m^{-1} s^{-1} is shown in Fig. 10. For Q_{1min} and Q_{30min}, the most frequent r_{u*t} values are now respectively 0.99 and 0.85, somewhat smaller than the estimated values for the full set (Fig. 9). In comparison, the most frequent r_{c0} values are now respectively 0.30 and 0.29, three to four times smaller than for the case when the full set is considered (Fig. 9). This suggests that c_0 has a clear dependency on u_* and is smaller for smaller u_*. This is because saltation is more intermittent in the case of smaller u_* (i.e. smaller excess shear stress) and thus, c_0, a descriptor of the relation between time-averaged saltation flux and friction velocity, is smaller for more intermittent saltation.

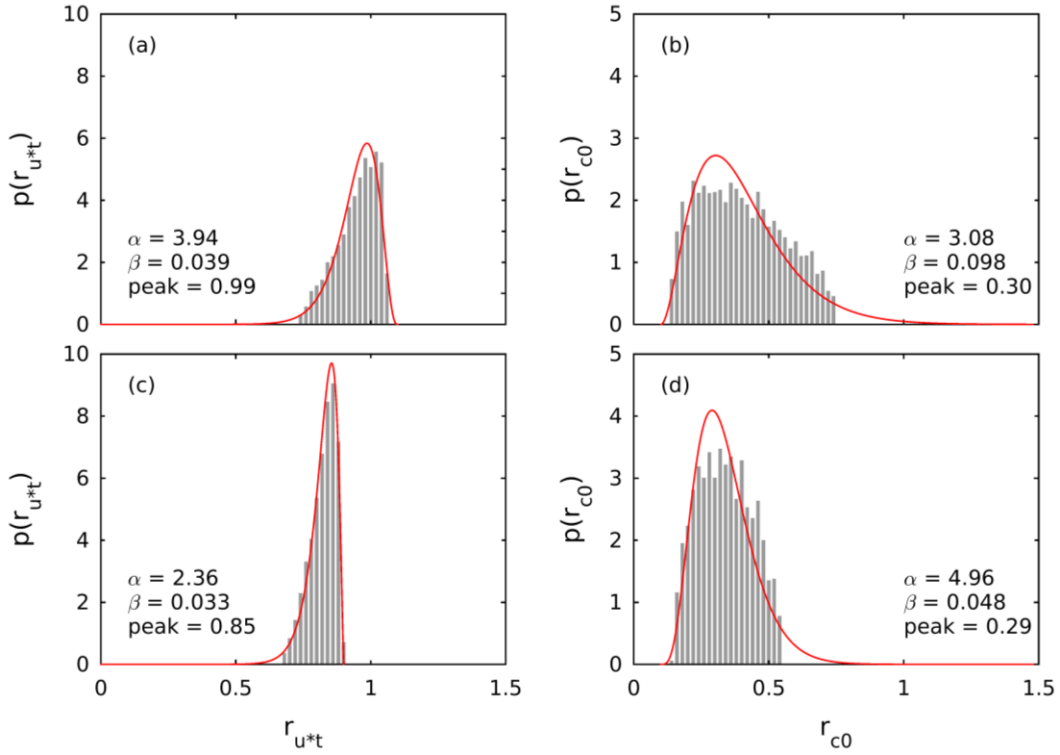

Figure 10: As Fig. 9, but estimated using the time series of saltation fluxes which satisfy $Q_{D,i} \leq 3$ g m^{-1} s^{-1}.

We fit the pdfs, $p(r_{u*t})$ and $p(r_{c0})$, for individual particle size bins and found that the most frequent r_{u*t} values do not differ substantially among the particle sizes, but r_{c0} depends systematically on particle size. For example, the most frequent r_{c0} values for 101, 151, 203, 315 and 398 µm are, respectively, 0.5, 1.3, 1.7, 3.1 and 4.0. These values are obtained by first estimating $p(r_{c0})$ for the individual particle size bins with the measured saltation flux for the corresponding bins and then normalizing $p(r_{c0})$ with the mass fraction of the size bins of the parent soil. A least squares curve fitting shows that the most frequent r_{c0} value depends almost perfectly ($R^2 = 0.996$) linearly on particle size:

$$r_{c_0} = 0.012d - 0.59 \qquad (15)$$

for the particle size range (100 to 400 µm) we tested, with d being particle size in µm.

We have shown that both u_{*t} and c_0 satisfy certain pdfs that depend on the properties of the surface, atmospheric turbulence and soil particle size. Fig. 9 shows that for a fixed choice of u_{*t} and c_0, even if they are "optimally" chosen, a portion of the measurements cannot be represented by the model. Then, how does the saltation model perform if a single fixed u_{*t} and a single fixed c_0 are used as is often the case in aeolian models? The $p(Q)$ computed using the model and derived from the JADE measurements are shown for Q_{1min} and Q_{30min} in Fig. 11. The model is applied to estimate the saltation flux for individual particle size groups using the optimally estimated u_{*t} and c_0 (with $r_{u*t} = 1.12$ and $r_{c0} = 1.04$ for Q_{1min}, and $r_{u*t} = 1.04$ and $r_{c0} = 0.92$ for Q_{30min}) and the total saltation flux is computed by integration over all particle size groups, i.e., using Equation (3). Fig. 11 shows that for this option, the model over predicts the probability of large Q, but under predicts the probability of small Q, in both cases of Q_{1min} and Q_{30min}. Obviously, to better reproduce the Q_{1min} *and* Q_{30min} pdfs, more values of r_{u*t} and r_{c0} sampled from the parameter pdfs are required. We have therefore modelled Q_{1min} with other

choices of r_{u*t} (1.12 and 0.56) and r_{c0} (2.08, 0.01) and plotted the corresponding Q_{1min} pdfs as well as the averaged Q_{1min} pdf of the three simulations. Similarly, we performed Q_{30min} model simulations with other r_{u*t} (1.04) and r_{c0} (1.84) values and examined the Q_{30min} pdfs. With the additional choices of the r_{u*t} and r_{c0} values, the Q_{1min} and Q_{30min} pdfs can be better reproduced.

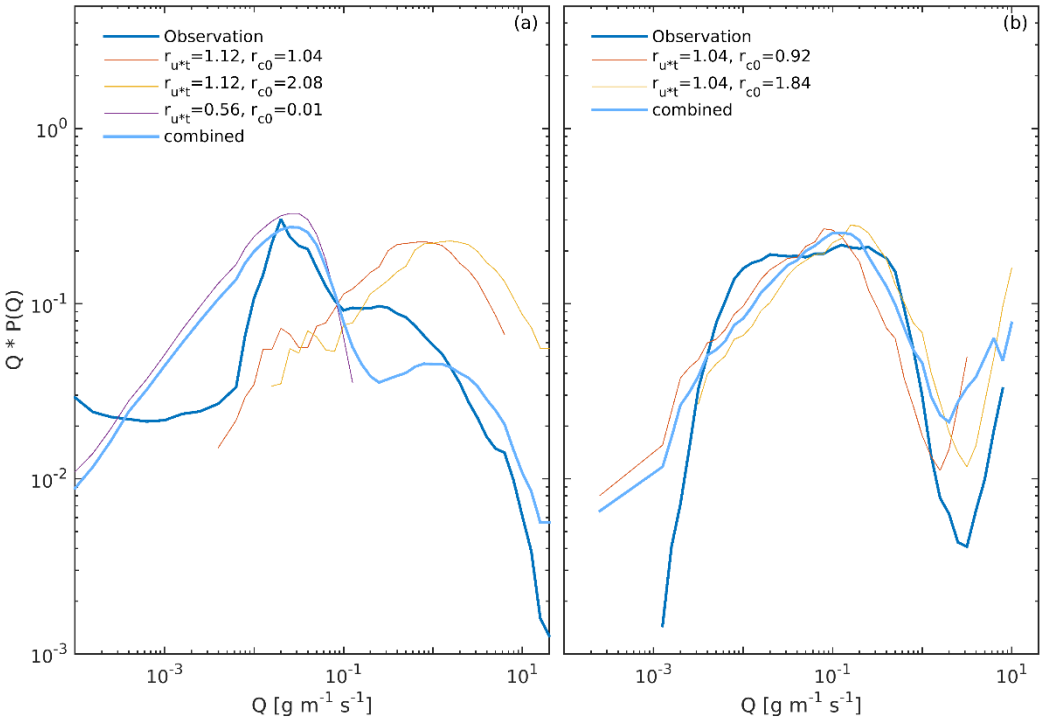

Figure 11: (a) Probability density functions of observed Q and simulated Q for 1-min averages with several choices of r_{u*t} and r_{c0}; (b) as (a), but for 30-min averages.

5. Summary

In this paper, we used the JADE data of saltation fluxes (resolution one second) and frictional velocity (resolution one minute) to analyze the statistical behavior of turbulent saltation and estimate the probability distribution of two important parameters in a saltation model, namely, the threshold friction velocity, u_{*t}, and saltation coefficient, c_0.

Saltation fluxes show rich variations on different scales. It is found that while the widely used $Q \sim u_*^3$ relationship holds in general, it can vary significantly between different wind erosion events. In several wind erosion events observed in JADE, saltation hysteresis occurred. We examined the probability density function of the saltation fluxes, $p(Q)$, and found that it generally behaves like $Q^{-\alpha}$ with $\alpha \sim 1$. For Q_{1sec}, there is a distinct change in α at $Q = 3 \sim 4$ g m^{-1} s^{-1} with $\alpha \sim 1$ for smaller Q and $\alpha \sim 4.0$ larger Q. It is shown that $p(Q)$ is dependent on the averaging time intervals as a consequence of saltation intermittency.

We introduced the saltation intermittency functions $\gamma_a(u_{*t})$, $\gamma_b(u_*)$ and redefined saltation intermittency γ_c as the fraction of time during which saltation occurs at a given point in a given time period, and computed these saltation intermittency measures using the JADE saltation flux measurements. It is found that $\gamma_a(u_{*t})$ is one at $u_{*t} = 0$ and decreases to zero at about $u_{*t} = 0.5$ ms^{-1}. For $u_{*t} = 0.2$ ms^{-1}, γ_a is 0.35. For Q_{1min}, , $\gamma_b(u_*)$ increases from about 0.6 at $u_* \sim 0.1$ ms^{-1} to about one at $u_* = 0.3$ ms^{-1}. This shows that a considerable fraction of the saltation fluxes occurs at small friction velocity and saltation is more intermittent under weak wind conditions

and is almost non-intermittent for $u_* > 0.3$ m s^{-1}. It is found that $\gamma_b(u_*)$ increased with decreasing u_* for $u_* < 0.1$ ms^{-1} which is unexpected. Overall, γ_c is found to be around 0.73. We computed γ_c as function of particle size and found that $\gamma_c(d)$ decreases with d, i.e., the saltation of larger particles is more intermittent. Also, $\gamma_c(d)$ increases with increased averaging time intervals, implying that the small scales features of turbulence play an important role in intermittent saltation.

The power spectra of Q and u_* are found to have qualitatively similar behaviour. Both have a maximum at about 10^{-5} Hz, a minimum at about 10^{-4} Hz and another peak at about $2\text{x}10^{-3}$ Hz. The maximum at 10^{-5} Hz is related to the diurnal to synoptic events that drive wind erosion episodes, the minimum at 10^{-4} Hz is due to the lack of turbulent wind fluctuations at the time scale of several hours, while the peak at $2\text{x}10^{-3}$ Hz is caused by minute-scale gusts/large eddies in turbulent flows. The power of the saltation rapidly decreases with frequency and becomes relatively weak at frequencies of 0.1 Hz.

The posterior pdfs of the two parameters were estimated using the DREAM algorithm applied to the JADE saltation flux measurements. While both u_{*t} and c_0 have clear physical interpretations, they are both stochastic parameters satisfying certain parameter pdfs. They also dependent on the intervals of time averaging. Both u_{*t} and c_0 for Q_{1min} are larger than for Q_{30min}. The pdf of u_{*t} shows that it has a most frequent value close to the theoretical value, but can vary over a range of 20% to 30%.The pdf of c_0 shows scatter over a wide range and it is unlikely that a universal c_0 exists. In a saltation model, even if the optimally estimated c_0 is used, considerable scatter between the model and the data would remain. The likely reason for the stochasticity in u_{*t} may be the temporal and spatial variations of particle cohesion, surface roughness, particle shape etc. which cannot be well represented by a fixed deterministic value, and the relatively large uncertainty in c_0 may be that this parameter depends on additional factors (e.g. u_* and soil particle size distribution) and is related to the fluctuations and intermittency of saltation. It may also be that saltation in reality is never in equilibrium as Bagnold (1941), Kawamura (1964) and Owen (1964) conceptualized, because due to turbulence, sand grains are continuously entrained at different rates into the airflow and a continuous flow- and particle-motion feedback takes place. As a consequence, it is difficult to treat c_0 as a universal constant.

In this study, we highlighted the need to better understand saltation as a turbulent process and the stochasticity of saltation model parameters. The concept of threshold friction velocity as a stochastic variable was put forward in Shao (2001). Raffaele et al. (2016) examined the pdf of u_{*t} using data compiled from publications. Raffaele et al. (2018) studied how u_{*t} uncertainties propagate in saltation flux calculations and reported that in the case of small excess shear stress, all models they tested amplify the uncertainty in estimated saltation flux, especially for coarse sand. This finding is consistent with our notion that c_0 also is a stochastic variable. Due to the stochasticity of the model parameters, the saltation model cannot reproduce the observation even with the optimally estimated parameters (e.g. under estimation of weak saltation fluxes and over estimation of strong saltation fluxes). A combination of several pairs of model parameters appears to be required to reasonably reproduce the pdfs of saltation fluxes.

Our estimates of the parameter uncertainties is based on the data of a relatively simple aeolian surface. For more complex surfaces, we expect the parameter uncertainties to be even more pronounced.

Acknowledgement: This research is funded by the National Natural Science Foundation of China (No. 41571090, 41201539). The data used in this study were obtained in JADE (the Japan Australian Dust Experiment) by M. Ishizuka, M. Mikami, J. F. Leys, Y. Yamada, and S. Heidenreich. We are grateful to P. Schlüter and Q. Xia for support with data processing. We also wish to thank Dr. J. Gillies, Dr. M. Klose and an anomalous referee for their very helpful comments which prompt us to rework on a number of issues presented in the first version of the paper.

References:

Anderson, R. S. and P. K. Haff (1988): Simulation of Eolian Saltation. Science 241, 820-823. DOI: 10.1126/science.241.4867.820

Bagnold, R.A. (1941): The Physics of Blown Sand and Desert Dunes. Methuen, London, 265pp

Butterfield, G. R. (1991): Grain transport rates in steady and unsteady turbulent airflows. Acta Mechanica, Suppl. 1, 97-122

Davidson-Arnott, R. G. D., and B. O. Bauer (2009): Aeolian sediment transport on a beach: Thresholds, intermittency, and high frequency variability. Geomorphology 105: 117–126

Dupont, S., G. Bergametti, B. Marticorena, and S. Simoëns (2013), Modeling saltation intermittency, J. Geophys. Res. Atmos., 118, 7109–7128, doi:10.1002/jgrd.50528

Ellis, J. T., D. Sherman, E. J. Farrell and B. L. Li (2012): Temporal and spatial variability of aeolian sand transport: Implications for field measurements. Aeolian Research 3(4):379-387. DOI: 10.1016/j.aeolia.2011.06.001

Fecan, F., Marticorena B., Bergametti G. (1999) Parametrization of the increase of the aeolian erosion threshold wind friction velocity due to soil moisture for arid and semi-arid areas. Annales Geophysicae 17:149–157

Gillette, D.A., E. Hardebeck and J. Parker (1997) Large-scale variability of wind erosion mass flux rates at Owens Lake 2. Role of roughness change, particle limitation, change of threshold friction velocity, and the Owen effect. J. Geophys. Res. 102, 25,989-25,998

Ishizuka, M., Mikami, M., Leys, J. F., Yamada, Y., Heidenreich, S., Shao, Y., McTainsh, G. H. (2008): Effects of soil moisture and dried raindroplet crust on saltation and dust emission. J. Geophys. Res. 113, D24212, doi:10.1029/2008JD009955

Ishizuka, M., Mikami, M., Leys, J. F., Shao, Y., Yamada, Y. and Heidenreich, S. (2014): Power law relation between size-resolved vertical dust flux and friction velocity measured in a fallow wheat field. Aeolian Research 12:87-99. DOI: 10.1016/j.aeolia.2013.11.002

Klose, M., Y. Shao, X. Li, H. Zhang, M. Ishizuka, M. Mikami, and J. F. Leys (2014): Further development of a parameterization for convective turbulent dust emission and evaluation based on field observations. J. Geophys. Res. Atmos. 119, 10,441–10,457, doi:10.1002/2014JD021688

690 Kok, J.F., N.M. Mahowald, G. Fratini, J.A. Gillies, M. Ishizuka, J.F. Leys, M. Mikami, M.S.
691 Park, S.U. Park, R.S. Van Pelt, T.M. Zobeck (2014): An improved dust emission model – Part
692 1: model description and comparison against measurements. Atmos. Chem. Phys. 14, 13023–
693 13041
694
695 Kawamura, R. (1964): Study of sand movement by wind. In: Hydraulic Eng. Lab. Tech. Rep.,
696 University of California, Berkeley, HEL-2-8, pp 99–108
697
698 Leys, J. F. (1998): Wind erosion processes and sediments in southeastern Australia. Ph.D.
699 Thesis, Griffith University, Brisbane
700
701 Namikas, S. L., B. O. Bauer and D. Sherman (2003): Influence of averaging on shear velocity
702 estimates for aeolian transport modeling. Geomorphology 53, 235-246, DOI: 10.1016/S0169-
703 555X(02)00314-8
704
705 McKenna-Neuman, C., N. Lancaster, and W. G. Nickling (2000): The effect of unsteady winds
706 on sediment transport on the stoss slope of a transverse dune, Silver Peak, NV, USA.
707 Sedimentology 47: 211–226
708
709 McNaughton, K. G. and J. Laubach (2000): Power Spectra and Cospectra for Wind and For
710 Wind and Scalars in a Disturbed Surface Layer at the Base of an Advective Inversion.
711 Boundary-Layer Meteorology 96: 143–185.
712
713 Owen, R. P. (1964): Saltation of uniform grains in air. J. Fluid. Mech. 20, 225–242
714
715 Raffaele, L., L. Bruno, F. Pellerey and L. Preziosi, 2016: Windblown sand saltation: A
716 statistical approach to fluid threshold shear velocity. Aeolian Research 23, 79–91,
717 http://dx.doi.org/10.1016/j.aeolia.2016.10.002
718
719 Raffaele, L., L. Bruno and G.F.S. Wiggs, 2018: Uncertainty propagation in aeolian processes:
720 From threshold shear velocity to sand transport rate. Geomorphology,
721 https://doi.org/10.1016/j.geomorph.2017.10.028
722
723 Raupach, M.R., Gillette D.A. and Leys J.F. (1993): The effect of roughness elements on wind
724 erosion thresholds. J. Geophys. Res. 98:3023–3029
725
726 Sadegh, M. and J. A. Vrugt (2014): Approximate Bayesian computation using Markov Chain
727 Monte Carlo simulation: DEARM$_{(ABC)}$. Water Resour. Res. 50, doi:10.1002/2014WR015386
728
729 Shao, Y. and Lu H. (2000): A simple expression for wind erosion threshold friction velocity. J.
730 Geophys. Res. 105:22,437–22,443
731
732 Shao, Y. (2001): Physics and Modelling of Wind Erosion. 1st Edition, Kluwer Academic
733 Publishers.
734
735 Shao, Y., M. Ishizuka, M. Mikami, and J. F. Leys (2011): Parameterization of size-resolved
736 dust emission and validation with measurements. J. Geophys. Res., 116, D08203,
737 doi:10.1029/2010JD014527
738

Shao, Y. and Mikami, M. (2005): Heterogeneous Saltation: Theory, Observation and Comparison. Boundary-Layer Meteorol. 115:359. doi:10.1007/s10546-004-7089-2

Sherman, D., B. L. Li, J. T. Ellis and C. Swann (2017): Intermittent aeolian saltation: A protocol for quantification. Geographical Review 1–19. DOI: 10.1111/gere.12249

Storn, R. and Price, K. (1997): Differential Evolution – a simple and efficient heuristic for global optimization over continuous spaces. J. Global Optim. 11, 341-359

Stout, J. E. and T. M. Zobeck (1997): Intermittent saltation. Sedimentology 44, 959-970

Stull, R. B. (1988): An Introduction to Boundary Layer Meteorology. Kluwer Academic Publishers.

Vrugt, J. A., ter Braak, C. J. F., Diks, G. H., Robinson, B. A., and Hyman, J. M. (2011): Accelerating Markov Chain Monte Carlo Simulation by Differential Evolution with Self-Adaptive Randomized Subspace Sampling. Int. J. Nonlin. Sci. Num. 10(3), 273-290doi:10.1515/IJNSNS.2009.10.3.273

Vrugt, J. A. and M. Sadegh (2013): Toward diagnostic model calibration and evaluation: Approximate Bayesian computation. Water Resour. Res. 49, 4335-4345. doi:10.1002/wrcr.20354

White, B.R. (1979): Soil transport by winds on Mars. J. Geophys. Res. 84, 4643-4651

Yamada Y., Mikami M., Nagashima H. (2002): Dust particle measuring system for streamwise dust flux. J. Arid Land Studies 11(4): 229–234